ACS SENSORS

Article

Cite This: ACS Sens. 2019, 4, 717−725

pubs.acs.org/acssensors

In Vivo Detection and Absolute Quantification of a Secreted Bacterial Factor from Skin Using Molecularly Imprinted Polymers in a Surface Plasmon Resonance Biosensor for Improved Diagnostic Abilities

Gizem Ertürk Bergdahl,*[,†] Tilde Andersson,[†] Maria Allhorn,[†] Sofie Yngman,[‡] Rainer Timm,[‡] and Rolf Lood[†]

[†]Division of Infection Medicine, Department of Clinical Sciences and [‡]Division of Synchrotron Radiation Research, Department of Physics, Lund University, 221 00 Lund, Sweden

Supporting Information

ABSTRACT: In this study, a surface plasmon resonance (SPR) biosensor was developed for the detection and quantification of a secreted bacterial factor (RoxP) from skin. A molecular imprinting method was used for the preparation of sensor chips and five different monomer-cross-linker compositions were evaluated for sensitivity, selectivity, affinity, and kinetic measurements. The most promising molecularly imprinted polymer (MIP) was characterized by using scanning electron microscopy, atomic force microscopy, and cyclic voltammetry. Limit of detection (LOD) value was calculated as 0.23 nM with an affinity constant of 3.3×10^{-9} M for the promising MIP. Besides being highly sensitive, the developed system was also very selective for the template protein RoxP, proven by the calculated selectivity coefficients. Finally, absolute concentrations of RoxP in several skin swabs were analyzed by using the developed MIP-SPR biosensor and compared to a competitive ELISA. Consequently, the developed system offers a very efficient tool for the detection and quantification of RoxP as an early indicator for some oxidative skin diseases especially when they are present in low-abundance levels (e.g., skin samples).

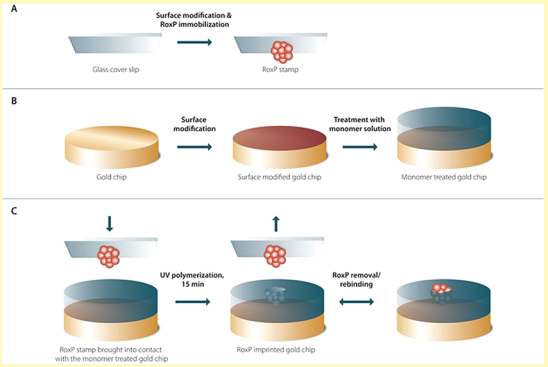

KEYWORDS: *surface plasmon resonance biosensor, secreted bacterial factor, molecular imprinting, competitive ELISA, oxidative skin diseases*

The role of the microbiota, e.g., the commensal microbes inhabiting our bodies, in health and in disease is a widely studied field, in part due to the impact of microbial dysbiosis for development of pathogenesis.[1,2] Most of the conducted studies have relied on studying modifications within bacterial populations, affecting the ratio of a bacterial species within a microbial population.[3,4] Similar data sets have enabled us to understand the impact of dysbiosis in several skin diseases, including psoriasis and atopic dermatitis.[5−7] These diseases are characterized by a high abundance of *Staphylococcus aureus* as well as a low ratio of *Propionibacterium* (*Cutibacterium*) *acnes*.[8] In particular, the low abundance of *P. acnes* has been suggested to be involved in their predisposition for developing skin diseases based on oxidative stress, due to *P. acnes*' potent secreted antioxidant RoxP being less prevalent in these patient groups.[9] RoxP, being a ca. 15 kDa (pI 7−10 depending on genotype) highly secreted bacterial protein on the skin, was recently described to be of importance for *P. acnes* colonization of skin.[10] While potent antioxidant activity has been attributed to the protein,[10] the molecular mechanism behind this activity has not yet been elucidated. A follow-up study investigated the prevalence of RoxP on skin *in vivo*, demonstrating skin disease specific levels of RoxP with medium prevalence of RoxP in actinic keratosis and high prevalence in basal cell carcinoma as compared to healthy individuals, as well as a general reduction of RoxP in disease affected skin compared to healthy skin.[9] The changes in protein quantities correlated well with microbial dysbiosis, with a reduced abundance of *P. acnes* in active oxidative stress diseases (e.g., actinic keratosis), and a higher level of high-RoxP producing *P. acnes* phylotypes in basal cell carcinoma.[9,10] As such, RoxP can function as a biomarker for skin oxidative stress on skin and was recently shown to be correlated with different skin pathologies (e.g., actinic keratosis and basal cell carcinoma).[9]

Conventional biomarker detection technologies such as ELISA, radio-immunoassay, or blotting techniques are generally very slow, expensive, not suitable for point-of-care applications, have a limited sensitivity and selectivity, and require the collection, labeling, and analysis of the samples by skilled

Received: December 21, 2018
Accepted: February 13, 2019
Published: February 13, 2019

DOI: 10.1021/acssensors.8b01642
ACS Sens. 2019, 4, 717−725

personnel.[11−13] Therefore, biosensors offer a very good alternative to these techniques thanks to their advantages of being fast(er), cost-efficient, sensitive, and label-free, as well as having the potential for miniaturization and therefore being more suitable for point-of-care applications. However, biosensors which rely on the use of biological molecules as biorecognition receptors suffer from some drawbacks.[14,15] Besides having very high affinity for their targets, these natural receptors are expensive, their production mainly requires complex procedures, such as the use of animals for antibody production, they have limited shelf life and stability, and they are not resistant to harsh conditions.[16]

In order to overcome these disadvantages originating from natural receptors, artificial receptors (e.g., molecularly imprinted polymers (MIPs)) may be a good alternative for biosensor applications. These polymers (MIPs) possess recognition cavities which are complementary to the template in their size, shape, and surface chemistry. Therefore, they exhibit a memory for the template itself. They have several advantages in their lower cost; reusability; thermal, mechanical, and chemical stability; easy production; long shelf life; and comparable binding kinetics to antibodies.[17−19] The process of generating the MIPs can be further facilitated by adsorbing the target protein on a glass surface, using this protein stamp to create imprints on a gold surface.[20,21] By this way, the binding sites are more accessible and mass transfer is faster.[22]

We recently developed a MIP-based capacitance biosensor for the detection of RoxP in complex skin samples.[21] Despite its high sensitivity and selectivity, we experienced significant fluctuations in the signals derived from the capacitance biosensor, resulting in significant standard deviations and less robustness. Here, we developed a novel biosensor application for RoxP based on a highly optimized and validated MIP analyzed in a surface plasmon resonance biosensor (SPR).

MATERIALS AND METHODS

Materials and Reagents. RoxP was recombinantly expressed in yeast to a high purity (>95% as judged by SDS-PAGE), and diluted to a stock concentration of 2 mg/mL.[9] Tyramine (99%, $HOC_6H_4CH_2CH_2NH_2$), acryloyl chloride, triethylamine, glutaraldehyde (25%, w/v), 3-amino-propyl-triethoxysilane (APTES), keratin from human epidermis, collagen from bovine Achilles tendon, chondroitin sulfate A sodium salt from bovine trachea, fibronectin from human plasma, human serum albumin, 2-hydroxyethyl methacrylate (98%) (HEMA), *N*-(hydroxymethyl)acrylamide solution (NHMA), poly(ethylene glycol) dimethacrylate (average Mn 550) (PEGDMA), *N*-isopropylacrylamide (NIPAM), acrylamide (AAm), and 1,1′-azobis (cyclohexanecarbonitrile) were purchased from Sigma-Aldrich. All buffers were prepared with water processed using a Milli-Q system from Millipore (Bedford, MA, USA), and prior to use, all buffers were filtered through a Millipore filter (pore size: 0.2 μm).

Instrumentation and Apparatus. Biacore X100 (GE Healthcare, Uppsala, Sweden) was used for protein binding assays, kinetic measurements, selectivity analysis, and RoxP detection from human skin swab samples. Bare gold sensor chips (SIA kit, Au) were obtained from GE Healthcare, Uppsala, Sweden. Ivium Compactstat (Ivium Technologies, Netherlands) with a three-electrode electrochemical system, that was configured by connecting the gold chip as working electrode, an Ag/AgCl reference electrode, and a platinum counter electrode, was used for electro-polymerization of tyramine on gold chips and for the characterization of the sensor surface. Surface characterization of the reference chip and modified gold sensor chips was carried out by using atomic force microscopy (JPK NanoWizard II) and scanning electron microscopy (Jeol JSM-7800F FEG-SEM).

Preparation of the Sensors. For the preparation of protein (RoxP) immobilized glass supports, in the first step, the glass slides were activated with 1 M NaOH by boiling them for 30 min. Then, the glass slides were immersed in 3-aminopropyl-triethoxysilane (3-APTES) in ethanol (10%, v/v) for 4 h at room temperature in order to introduce amino groups on the surface. In the following step, the amino groups on the surface were activated with 7% Glutaraldehyde (v/v) in 10 mM phosphate buffer (pH: 7.4) by immersing the glass slides for 2 h at room temperature in the mixture. In the last step, the glass slides were treated with the template protein solution (RoxP, 0.5 mg.mL^{-1}), which was prepared in 10 mM phosphate buffer (pH: 7.4), overnight at 4 °C. By this way, the template protein (RoxP) was immobilized on the glass slide surface to be used as the stamp in the further molecular imprinting process.

For the preparation of gold chips, in the first step, the chips were cleaned with ethanol (95%) and acidic piranha solution (3:1, H_2SO_4:H_2O_2, v/v), respectively, for 10 min in each step, in an ultrasonic cleaner. Then, the chips were rinsed with distilled water and dried with nitrogen gas. In the following step, electro-polymerization of tyramine was applied to the surface of the chips by using cyclic voltammetry in a 10 mM tyramine solution prepared in ethanol (95%) in order to introduce free primary amino groups on the surface. Then, the chips were immersed in a solution of 30 mM acryloyl chloride and 30 mM triethylamine, prepared in toluene, overnight at room temperature. By this way, the amide groups were generated on the surface and free vinyl groups were left to be involved in the following polymerization step. After rinsing the chips with distilled water and drying with nitrogen, they were ready to be used in the subsequent step.

In the last step, molecular imprinting was performed. First, monomer solutions containing different functional monomers (HEMA, NHMA, AAm, NIPAM) and cross-linker (PEGDMA) were prepared as follows: For the MIP-1 sensor: HEMA (100 μL), PEGDMA (500 μL) and MQ water (400 μL), MIP-2 sensor; HEMA (50 μL), NHMA (50 μL), PEGDMA (500 μL), and MQ water (400 μL); MIP-3 sensor: NIPAm (95.6 mg), AAm (54 mg), PEGDMA (500 μL), and MQ water (500 μL); MIP-4 sensor: NIPAM (95.6 mg), NHMA (50 μL), PEGDMA (500 μL), and MQ water (450 μL); and MIP-5 sensor: NHMA (100 μL), PEGDMA (500 μL), and MQ water (400 μL) were prepared in the presence of UV initiator (2.8 mg for all the MIPs). For the polymerization step, 1.3 μL of each monomer solution was dropped onto the pre-modified gold chips and the protein stamps were gently placed on top of them. Polymerization was started under UV-curing system (Dymax, 400 W, 365 nm) and continued for 15 min. At the end of the polymerization, the protein stamps were removed from the surface and the imprinted gold chips (MIPs 1−5) were analyzed for analyte detection, analyte selectivity, and kinetic measurements in the following steps.

A reference chip (non-imprinted, NIP chip) was also prepared as a control surface by using HEMA (100 μL), PEGDMA (500 μL), MQ water (400 μL), and UV-initiator (2.8 mg) in order to investigate non-specific binding and to compare the selectivity of the imprinted system. The exact same procedure was applied to the preparation of the reference chip as to the imprinted chips with the sole difference being the presence or absence of immobilized RoxP on the glass slide. Therefore, the reference chip did not contain any RoxP-specific cavities.

Characterization of the Sensors. *Scanning Electron Microscopy (SEM) Analysis.* Samples were mounted on a 25 mm aluminum stubs (Ted Pella) with a silver paint (Ted Pella) and allowed to dry overnight. Samples were then sputter coated (Quorum Q 150T ES) with 5 nm chromium and viewed immediately at high vacuum in a Jeol JSM-7800F FEG-SEM at 5 kV acceleration voltage.

Atomic Force Microscopy (AFM) Analysis. For AFM measurements, a JPK NanoWizard II operated in intermittent contact mode in air was used. A point Probe Plus Si-SPM-sensor from Nanosensors with a tip radius of curvature of less than 10 nm was used as a probe. This system was convenient for sub-nanometer vertical resolution.[23]

Cyclic Voltammetry (CV) Analysis. CV experiments were carried out by using a mobile electrochemical measurement station (Ivium CompactStat, Netherlands). For all electrochemical measurements, a Biacore gold chip was used as the working electrode, and a platinum and an Ag/AgCl electrode as the counter and reference electrode, respectively. A solution of 0.1 M KCl containing 0.1 M potassium

DOI: 10.1021/acssensors.8b01642
ACS Sens. 2019, 4, 717−725

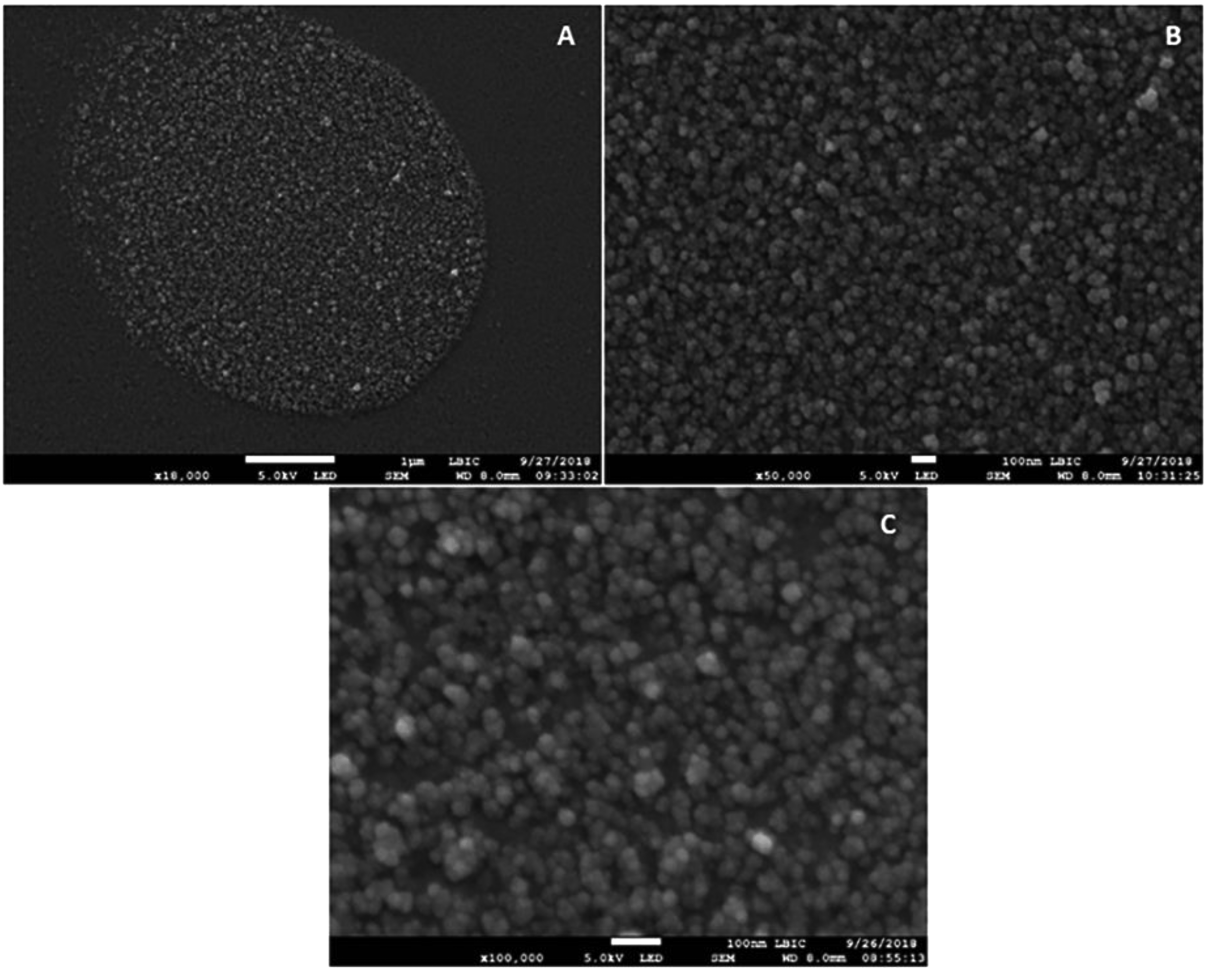

Figure 1. Characterization of the sensors. SEM images of RoxP-MIP1 sensor surface (A: 18 000×; B: 50 000×; C: 100 000×).

ferricyanide was used as the electrolyte solution. CV measurements were performed between the potential range of −0.3 V and +0.8 V at a scan rate of 0.1 $V.s^{-1}$.[24] CV measurements were performed after each modification step including bare gold surface, gold surface after UV polymerization.

Binding Analysis with the RoxP Imprinted Sensors. Standard RoxP solutions were prepared in the concentration range of 5.2×10^{-4} μM and 68 μM in running buffer (HBS-P; 0.01 M HEPES pH 7.4, 0.15 M NaCl, 0.05% v/v Surfactant P20) and injected into the Biacore X-100 system. Same standard solutions in different concentration ranges were tested for each imprinted chip (MIPs 1−5) in order to investigate sensitivity. All the assays were carried out at room temperature at a flow rate of 10 $\mu L.min^{-1}$.

A reference chip (e.g., non-imprinted) was also tested for binding analysis by using the standard RoxP solutions in order to determine non-specific binding.

Selectivity of the RoxP Imprinted Sensors. In order to determine the selectivity of the imprinted chips for RoxP, putatively interfering (cross-reactant) proteins including keratin, collagen, albumin, fibronectin, and chondroitin sulfate were injected into the system and tested for each imprinted chip (MIPs 1−5) in order to investigate selectivity for RoxP. The response of the system for the interfering proteins was compared with the response of the system for RoxP. The protein concentration for the selectivity analysis was 1.0 $mg.mL^{-1}$ for each protein.

The purpose of this study was to develop a method to quantitate RoxP on skin. Therefore, some of the most abundant skin proteins, as well as certain plasma proteins present during inflammation, leaking out from the blood vessels were tested for the selectivity experiments.

The response of the reference chip for the interfering proteins was also reported for the selectivity experiments in order to compare the selectivity of the imprinted system with a control (non-imprinted) one.

RoxP Detection from Human Skin Swab Samples. Healthy individuals were swabbed on a defined anatomical location (4 cm^2) for 30 s with a buffer pre-soaked swab (Venturi Transystem, Copan, Italy) for the isolation of RoxP. The skin swab was moved to a microcentrifuge tube with HBS-P (1 mL), and repeatedly stirred to release putative absorbed proteins. The sample was centrifuged (3500 g, 10 min) to remove cellular debris and skin swab residues. The remaining solution was sterile filtered (0.2 μm) before analysis with the biosensor using the RoxP-MIP1 chip. As a negative control, a swab directly put into the HBS-P microcentrifuge tube without swabbing the skin was used. Similarly, the calibration curve was established from such mock skin swab spiked with RoxP. The study was approved by the ethical committee in Malmö/Lund (2016/465), and in accordance with the Declaration of Helsinki. Written informed consent was obtained from all participants before enrollment.

Development of a Competitive Enzyme-Linked Immunosorbent Assay (ELISA) for Detection of RoxP. Microtiter plate (NUNC MaxiSorp, Thermo Scientific, Denmark) was coated with 100 μL of recombinant RoxP in PBS at a concentration of 5 $\mu g.mL^{-1}$ and incubated overnight at 4 °C. Next day, the plate was blocked with 150 μL, 1% BSA in PBS, and incubated for 2 h. Meanwhile, antigen−antibody mixture containing equal volumes of either RoxP in concentrations 118 $pg.mL^{-1}$ − 5 $\mu g.mL^{-1}$ (or sample with unknown concentration) and polyclonal antibody against RoxP (Agrisera, Sweden), diluted 1:500, were pre-incubated 2 h before addition of 100 μL of each mixture to the wells for continued incubation for 1 h. In the next step 100 μL of secondary antibody, swine-anti-rabbit IgG

DOI: 10.1021/acssensors.8b01642
ACS Sens. 2019, 4, 717−725

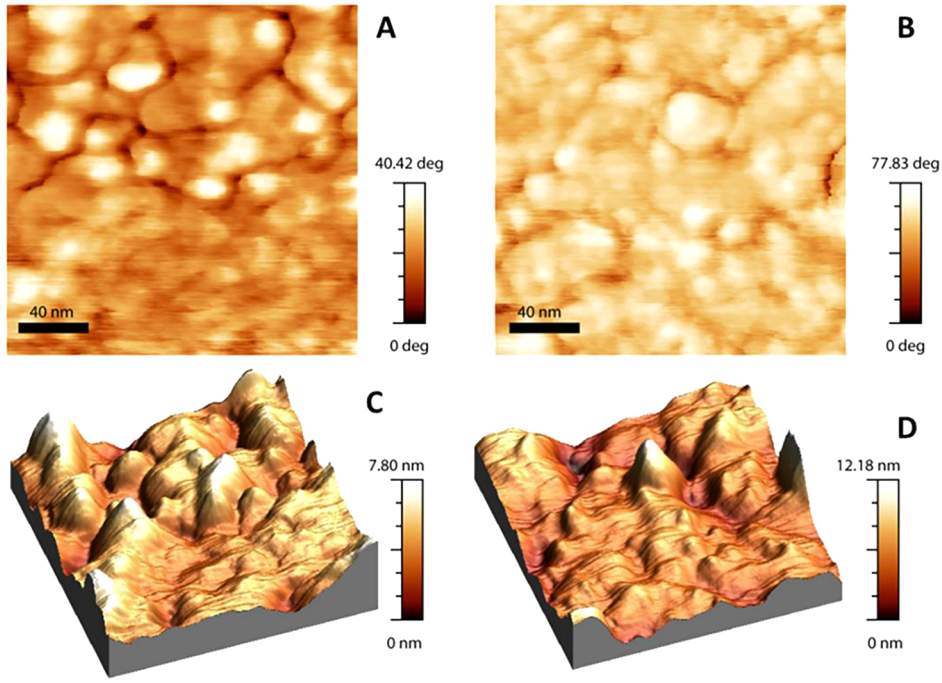

Figure 2. Characterization of the sensors. 2D representation of AFM phase image on (A) RoxP-imprinted sensor, (B) reference sensor; 3D representation of simultaneously acquired AFM height image on (C) RoxP-imprinted sensor, (D) reference sensor (Scanning area: 200 × 200 nm^2). The AFM phase signal is sensitive to local changes of the tip−sample interaction such as adhesion or energy dissipation, but it also enhances small-scale features of the sample topography.

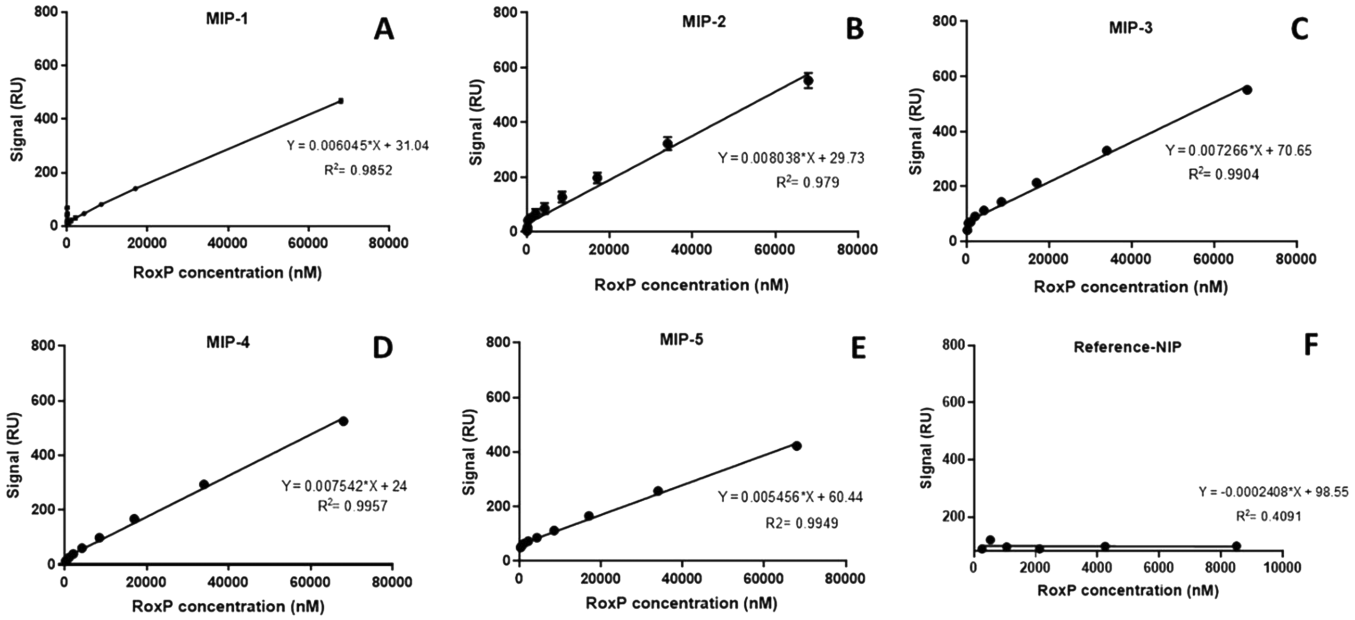

Figure 3. Binding Analysis. RoxP detection with RoxP-imprinted sensors. (A) MIP-1, (B) MIP-2, (C) MIP-3, (D) MIP-4, (E) MIP-5, and (F) Reference-NIP sensors. Using different concentrations of RoxP, calibration curves were established and fitted to the linear regression models in optimum conditions (running buffer: HBS-P; 0.01 M HEPES pH 7.4, 0.15 M NaCl, 0.05% v/v Surfactant P20, regeneration buffer: 10 mM glycine-HCl, pH: 2.5, flow rate: 10 $\mu L.min^{-1}$, T: 25 °C) (Triplicate analyses were performed for MIP-1 and MIP-2 sensors).

conjugated to horseradish peroxidase (Dako, Denmark), diluted 1:4000 was added and incubated for 1 h. Finally, 100 μL TMB substrate (Life Technologies, USA) was added until desired color change was attained (approximately 20−30 min). Absorbance was read at 450 nm after addition of stop solution. Three times repeated wash with 300 μL 0.05% Tween in PBS was included between each incubation step which were carried out at 37 °C unless otherwise stated.

RESULTS AND DISCUSSION

Characterization of the Sensors. The MIP-1 (HEMA-PEGDMA) sensor chip was used in the characterization studies.

SEM Analysis. In order to compare the surface morphology of the reference and the imprinted surfaces, we assessed the polymer structure on the chip using SEM. Bare and smooth gold surface on the reference chip (Figure SI-1) and a thin polymeric layer covering the gold chip with homogeneously distributed

DOI: 10.1021/acssensors.8b01642
ACS Sens. 2019, 4, 717−725

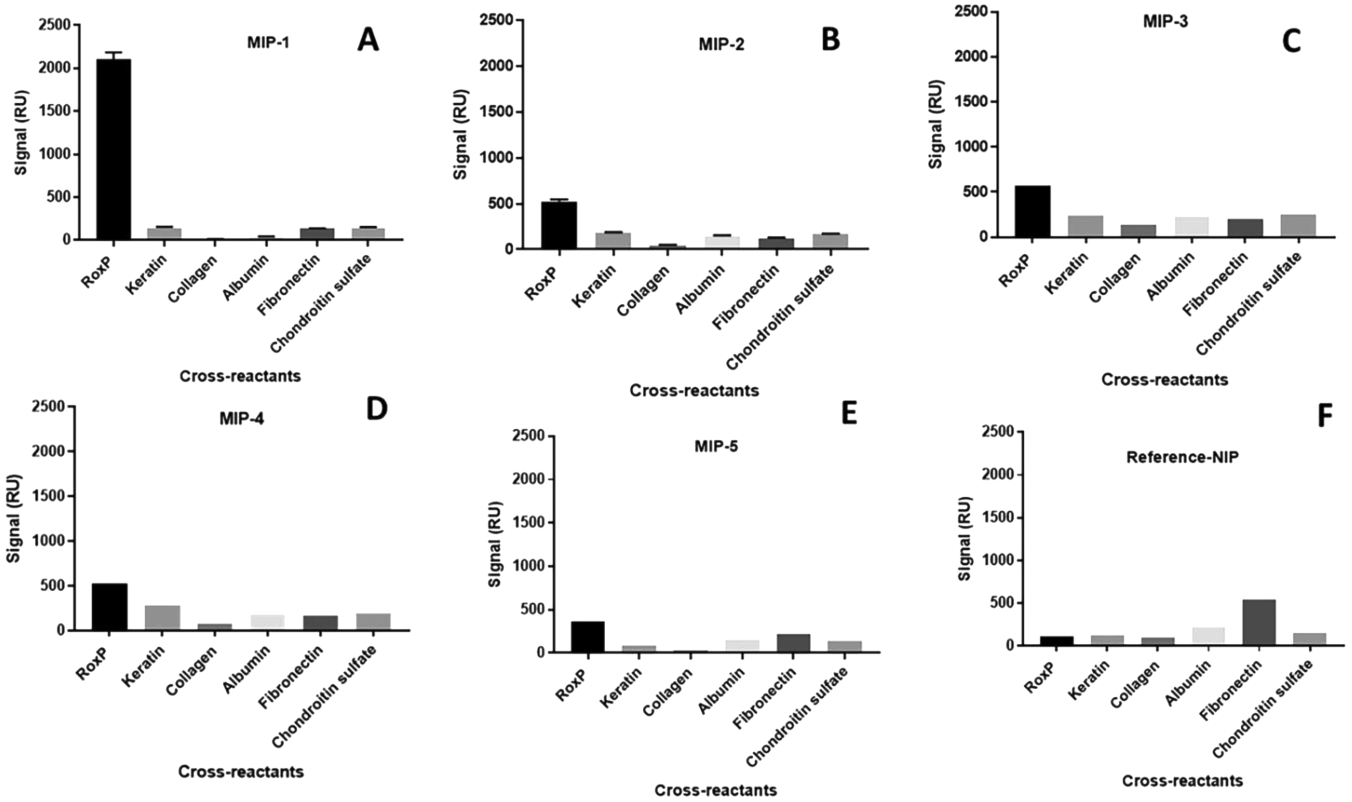

Figure 4. Selectivity Analysis. Selectivity of RoxP-imprinted (A) MIP-1, (B) MIP-2, (C) MIP-3, (D) MIP-4, (E) MIP-5, and (F) reference-NIP sensors for RoxP vs interfering proteins in optimum conditions (running buffer: HBS-P; 0.01 M HEPES pH 7.4, 0.15 M NaCl, 0.05% v/v Surfactant P20, regeneration buffer: 10 mM glycine-HCl, pH: 2.5, flow rate: 10 μL.min^{-1}, T: 25 °C) (Triplicate analyses were performed for MIP-1 and MIP-2 sensors).

cavities after imprinting can be visualized in different magnifications (Figure 1), indicating a successful formation of RoxP-imprinted cavities on the gold chip.

AFM Analysis. Due to the expected nanosized topographic differences between the imprinted and non-imprinted gold chips, we further performed a topographic analysis using AFM. The images of 200 nm × 200 nm (Figure 2) and 1 μm × 1 μm (Figure SI-2) large areas show the homogeneous distribution of the imprints. While not necessarily detectable in a 1 μm × 1 μm overview image, the higher resolution of the 200 nm × 200 nm large image allows for detection of 4−5 nm imprints, corresponding with the expected size of the template protein. This observation is also similar to what was observed in the SEM analysis (Figure 1). The imprinted chip displays lower roughness and corrugation, but larger lateral feature sizes, as compared to the non-imprinted chip. A similar phenomenon has been described earlier, with decreased roughness of the imprinted chip compared to the reference chip with no further explanation.[25] Possibly, the mechanical application of the protein-immobilized glass surface (as compared to non-immobilized glass surface) during polymerization may result in compression on the surface and thus result in smaller depths compared to the reference surface. To fully understand the mechanism behind this phenomenon, more experiments would be needed.

CV Analysis. To finally confirm the degree and quality of the gold surface being covered by the polymer, we performed cyclic voltammetry by using the permeable redox couple $K_3[Fe(CN)_6]$. In Figure SI-3, it can be seen that, compared to bare gold surface(a) the redox peaks disappeared after UV-polymerization (b) and coverage of the surface with the polymeric film resulted in a highly covered interface which can be seen from the fully blocked electron transfer. Taken together, the data indicates the successful coverage of the sensor surface with the polymer.

Binding Analysis with RoxP Imprinted Sensors. In order to assess whether the monomer compositions of the different constructed RoxP-MIP chips affected their functionality, we first investigated their ability to bind RoxP. All sensors were able to detect RoxP with a good correlation and good fitting to the linear regression, while the non-imprinted (NIP) chip did not result in increased signal (RU) with increased RoxP concentrations indicating that the signal increase in the MIPs were due to imprinted RoxP cavities (Figure 3 and Figure SI-5). However, MIP-1 and MIP-2 sensors had a much higher sensitivity than MIP-3, MIP-4, and MIP-5 sensors with a limit of quantification (LOQ) of 0.52 nM and 256.6 nM, respectively. The limit of detection (LOD; 3×SD from blank) was calculated to 0.23 nM and 2.08 nM for MIP-1 and MIP-2 sensors, respectively. The limit of detection (LOD) value was determined by calculating 3 times of the standard deviation of blank sample (buffer) and converting it into protein concentration from the calibration graph. As such, addition of HEMA increased the binding capacity of RoxP as compared to the other functional monomers (NIPAm, AAm, NHMA). Likewise, combining HEMA with NHMA (MIP-2) further reduced the binding response compared to HEMA alone. This can be attributed to the extensive swelling nature of the polymer (PHEMA) when it is subjected to water because of the presence of hydrophilic groups. In this way, it can increase the surface area

DOI: 10.1021/acssensors.8b01642
ACS Sens. 2019, 4, 717−725

Table 1. Selectivity Coefficients of RoxP Imprinted Sensors and the Reference Sensor[a]

A					
Cross-reactant	RU_{MIP-1}	k_{MIP-1}	RU_{NIP}	k_{NIP}	k'_{MIP-1}
RoxP	2092.7 ± 86.5	-	110.3	-	-
Keratin	142 ± 12.3	14.7 ± 7.06	117.9	0.9	15.8
Collagen	12.2 ± 0.7	171.5 ± 123.6	92.5	1.9	143.9
Albumin	40.4 ± 2.3	51.8 ± 38.5	220.8	0.5	103.7
Fibronectin	132.2 ± 8.2	15.8 ± 10.6	546.9	0.2	78.5
Chondroitin sulfate	144.1 ± 8.0	14.5 ± 10.9	158.1	0.7	20.8
B					
Cross-reactant	RU_{MIP-2}	k_{MIP-2}	RU_{NIP}	k_{NIP}	k'_{MIP-2}
RoxP	529.5 ± 21.7	-	110.3	-	-
Keratin	182.9 ± 6.1	2.9 ± 3.6	117.9	0.9	3.1
Collagen	48.4 ± 3.0	10.9 ± 7.5	92.5	1.9	9.2
Albumin	145 ± 9.1	3.7 ± 2.4	220.8	0.5	7.3
Fibronectin	116.9 ± 8.2	4.5 ± 2.7	546.9	0.2	22.5
Chondroitin sulfate	163.9 ± 10.1	3.2 ± 2.2	158.1	0.7	4.6
C					
Cross-reactant	RU_{MIP-3}	k_{MIP-3}	RU_{NIP}	k_{NIP}	k'_{MIP-3}
RoxP	576.2	-	110.3	-	-
Keratin	244.3	2.4	117.9	0.9	2.5
Collagen	134.3	4.3	92.5	1.9	3.6
Albumin	226.4	2.6	220.8	0.5	5.1
Fibronectin	202.4	2.9	546.9	0.2	14.1
Chondroitin sulfate	255.7	2.3	158.1	0.7	3.3
D					
Cross-reactant	RU_{MIP-4}	k_{MIP-4}	RU_{NIP}	k_{NIP}	k'_{MIP-4}
RoxP	524.6	-	110.3	-	-
Keratin	284.3	1.9	117.9	0.9	2.0
Collagen	74.1	7.1	92.5	1.9	5.9
Albumin	172.1	3.1	220.8	0.5	6.1
Fibronectin	169.7	3.1	546.9	0.2	15.3
Chondroitin sulfate	194.1	2.7	158.1	0.7	3.9
E					
Cross-reactant	RU_{MIP-5}	k_{MIP-5}	RU_{NIP}	k_{NIP}	k'_{MIP-5}
RoxP	361.1	-	110.3	-	-
Keratin	84.1	4.3	117.9	0.9	4.6
Collagen	34.6	10.4	92.5	1.9	8.8
Albumin	156	2.3	220.8	0.5	4.6
Fibronectin	213.7	1.7	546.9	0.2	8.4
Chondroitin sulfate	140.9	2.6	158.1	0.7	3.7

[a]RU_{MIP}: resonance unit/response of the imprinted sensors for the analytes, k_{MIP}: selectivity coefficient for RoxP versus cross-reactant proteins for the imprinted sensors, RU_{NIP}: resonance unit/response of the reference sensors for the analytes, k_{NIP}: selectivity coefficient for RoxP versus cross-reactant proteins for the reference sensors, k': selectivity of the imprinted sensors vs. reference sensor(Triplicate analysis were performed for MIP-1 and MIP-2 sensors. Standard deviations were reported on the table for these sensors).

and makes it more accessible for more RoxP binding.[26] In our previous study, the LOD value was reported as 25 attomolar (25×10^{-18} M) for RoxP when we used in a capacitive biosensor.[21] Though able to detect much lower levels of RoxP, its narrower dynamic range in combination with high standard deviation as a practical means of superior sensitivity decreases its robustness in a diagnostic setting. A biosensor as described herein (e.g., RoxP-MIP-1 analyzed in a surface plasmon resonance biosensor), though a lower sensitivity, offers an unmatched robustness and a broad dynamic range, able to detect RoxP concentrations of relevance for biological samples. The sensorgrams for MIP-1 which show the RoxP binding versus time are shown in Figure SI.4.

To further investigate the impact of the monomer composition for RoxP-interaction, binding kinetic constants were also investigated. The affinity constant (K_D) for all chips was calculated using a simple, one-to-one Langmuir model (SI Table 1). K_D values show the strength of the intermolecular interactions which means that a smaller K_D indicates a higher affinity between the ligand and the analyte. The MIP-1 chip had the lowest K_D value (3.3×10^{-9}) with an affinity more than 100× stronger than the other MIP compositions investigated. Most antibody−antigen interaction affinities vary between 10^{-6} and 10^{-12},[27] making the MIP-template interaction a high-affinity interaction.

Selectivity of the RoxP Imprinted Sensors. While sensitivity is of high importance for the development of a robust biosensor, the selectivity also needs to be on par. The selectivity of the imprinted sensors was tested against various proteins that are likely to be identified in skin samples together with RoxP

DOI: 10.1021/acssensors.8b01642
ACS Sens. 2019, 4, 717−725

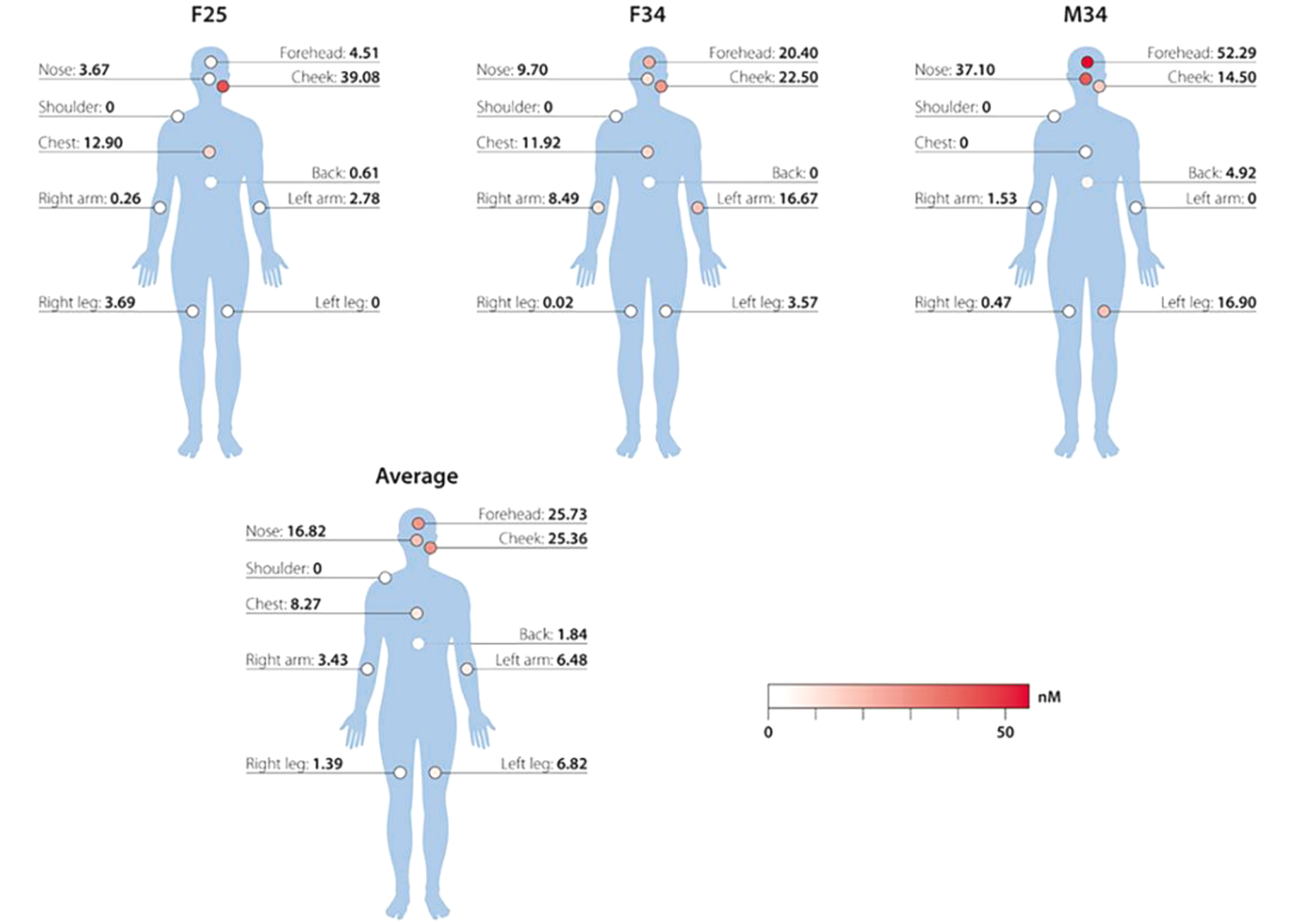

Figure 5. Heat-map skin sample analysis. RoxP detection from different skin parts of three different individuals (F25, F34, and M34; F/M indicating gender and number age) by using RoxP-imprinted (MIP-1) sensor. All values are given as mean of a triplicate and expressed in nM RoxP.

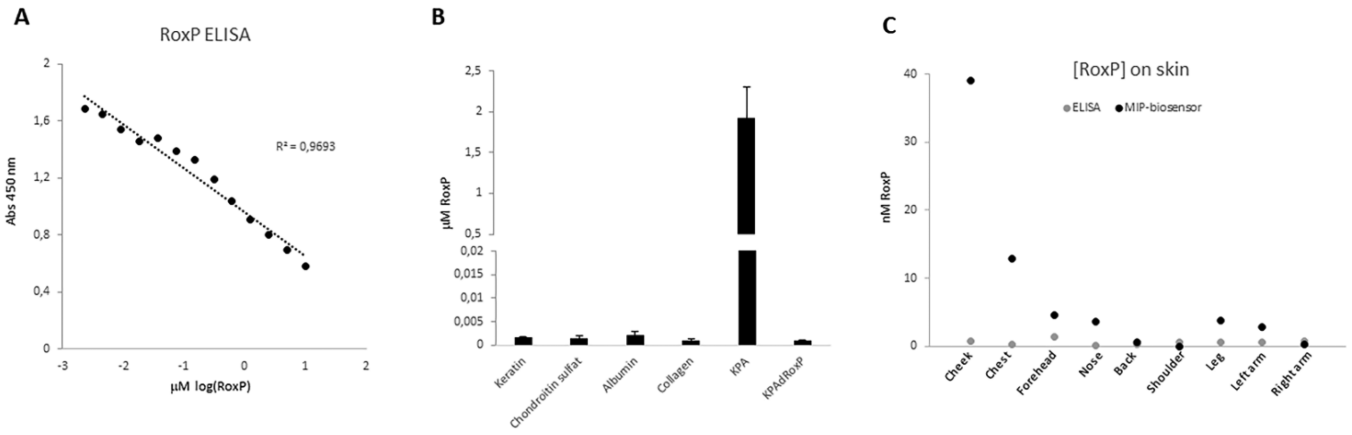

Figure 6. Development of a competitive RoxP ELISA. (A) Standard curve with plotted concentration of RoxP with μM RoxP on x-axis and absorbance unit on the y-axis of the graph. A trend line was fitted ($R^2 = 0.9693$) with a logarithmic fit, and concentrations of unknowns were interpolated from the standard curve. (B) Analysis of cross-reactivity of the anti-RoxP antibody with human proteins (keratin, chondroitin sulfate, albumin, and collagen; 150 ng.mL^{-1}) as well as against a bacterial supernatant from *P. acnes* strain KPA171202 and its isogenic RoxP mutant. (C) Screening of the RoxP concentrations in swab specimens collected from different human skin parts, as indicated in the figure, using competitive ELISA as compared to a MIP-biosensor approach (Average of three measurements were presented on the figure).

during different skin pathologies, including keratin, collagen, human serum albumin, fibronectin, and chondroitin sulfate. Molecular sizes and isoelectronic points (pIs) of the proteins used in selectivity analysis are shown in SI Table 2. The comparison of the sensor's response for the proteins for all the imprinted chips and for the reference chip and the calculated selectivity coefficients is shown in Figure 4 and Table 1, respectively. Interestingly, addition of HEMA to the polymer structure adds not only increased sensitivity but also increased selectivity, making the MIP-1 chip the most selective of all the

DOI: 10.1021/acssensors.8b01642
ACS Sens. 2019, 4, 717−725

different imprinted polymers. The reference sensor could not distinguish between the different proteins, giving similar signal intensities regardless of template (Figure 4). Although the reference chip contains various functional groups on the surface, it does not contain defined cavities which promotes the selective binding of RoxP. The imprinted chips contain specific recognition sites which are complementary to the template in size, shape, and positioning of the functional groups which provide the selective template binding as seen in the figure (Figure 4).

When the results are compared with reported selectivity results for RoxP that we obtained from our previous report,[21] we can detect RoxP with a significantly improved selectivity using the monomer composition developed herein (e.g., MIP-1). Previous selectivity coefficients (k values) increased from 3.60 to 171.5 for collagen, and from 5.14 to 51.8 for albumin. While designing MIPs for the target analytes, the monomer types and the composition thereof have important effects on the selectivity and sensitivity of the imprinted polymers.

RoxP Detection from Human Skin Swab Samples. After identifying MIP-1 as the most sensitive and selective chip in our investigation, we used the biosensor to perform absolute quantification of RoxP from skin swabs including different anatomical locations of the skin from three healthy individuals (Figure 5). There was no significant difference in RoxP quantities between the individuals as analyzed by ANOVA (Table SI-3). The observed values are in agreement with both expected values on the skin (as extrapolated from colonization numbers of *P. acnes*)[28] and in anatomic distribution with the highest value in sebum rich areas (see SI), suggesting that the biosensor is able to detect and accurately quantitate RoxP levels *in vivo* in complex environments despite the "contamination" with highly abundant skin proteins.

Comparison of the Detection Performance of the Method with ELISA. To allow for a more high-throughput quantification of RoxP on skin, we developed an ELISA based on competitive detection of RoxP using RoxP-specific antibodies (Figure 6A). While competitive ELISAs are preferable for complex material with high concentrations of contaminating proteins (e.g., skin swabs), they suffer in sensitivity as compared to other ELISAs.[29] While we could measure signals down to single nM quantities of our substrate (Figure 6A), the background signal often reached levels corresponding to >5 nM RoxP quantities (data not shown), indicating that low nM concentrations are close to undetectable using this ELISA setting. Similarly, too high concentrations of RoxP cannot be measured due to the competitive nature of the methodology.[29] Despite slight limitations in sensitivity, the selectivity for the ELISA was comparable or better than the MIP-1 chip (Figure 6B) and was an efficient tool for the detection and quantification of RoxP levels in bacterial culture supernatants (Figure 6B), allowing it to be useful for high-throughput screening of cultures for RoxP expression.

However, for the quantification of low-abundance levels of RoxP (e.g., patient samples, skin swabs), the limited detection level of the ELISA is detrimental. While the biosensor could quantitate the prevalence of RoxP on skin with high resolution, all values for the ELISA were barely higher than the control, thus resulting in a low-resolution mapping of the quantities (Figure 6C). The data from the MIP-1 biosensor displays an anatomic localization-dependent expression of RoxP similar to the distribution of *P. acnes* on skin (e.g., high levels in sebaceous rich regions), while the ELISA data fails to show any such biological variance on the skin. Consequently, in the presence of high concentrations of RoxP in samples, necessitating a high-throughput assay, the competitive RoxP-ELISA developed herein is highly useful. However, for the quantification of low-abundance levels of RoxP, a biosensor system, with its superior sensitivity, high reusability (>500 analyses per sensor chip), and fast, real-time, and label-free analysis offers a more efficient tool.

CONCLUSION

Herein, we developed a surface plasmon resonance biosensor for detecting a secreted bacterial protein (RoxP) as an early indicator for oxidative skin diseases. We used a type of surface imprinting method which is, to our knowledge, for the first time implemented to Biacore systems. By using this method, we immobilized the template protein on a solid surface which was then used as the protein stamp in the molecular imprinting process. By this way, we detected RoxP in a highly sensitive (KD: 3.3×10^{-9} M; LOD: 0.23 nM) and selective way which brought the possibility of detecting and quantifying the protein in skin samples even though it was very low abundant compared to interfering proteins. Comparison of the method with ELISA showed the strength of both techniques for different purposes: ELISA for high-throughput; MIP biosensors for increased sensitivity and higher resolution. Therefore, the developed system can be used as a model proof-of-concept for a powerful tool for the detection of low abundant biomarkers which are important for the early diagnosis of diseases.

ASSOCIATED CONTENT

Supporting Information

The Supporting Information is available free of charge on the ACS Publications website at DOI: 10.1021/acssensors.8b01642.

Data showing detailed characterization of the sensor surface, real-time sensorgrams that show the binding of the analyte, affinity constants, information regarding cross-reactant molecules which were used in the selectivity experiments and statistical analysis for the skin samples (PDF)

AUTHOR INFORMATION

Corresponding Author

*E-mail: gizem.erturk_bergdahl@med.lu.se.

ORCID

Gizem Ertürk Bergdahl: 0000-0001-9719-6609

Rainer Timm: 0000-0001-8914-5924

Author Contributions

All authors have given approval to the final version of the manuscript.

Notes

The authors declare no competing financial interest.

ACKNOWLEDGMENTS

This work was supported by grants from the Royal Physiographic Society of Lund, the Swedish Society for Medicine, and the foundations of Crafoord, Längmanska Kulturfonden, Alfred Österlund, Tornspiran, Magnus Bergvall, Åke Wiberg, Clas Groschinsky, Swedish Research Council and Sigurd and Elsa Goljes Minne. Lund University Bioimaging Center (LBIC), Lund University, is gratefully acknowledged for providing experimental resources (scanning electron microscopy).

DOI: 10.1021/acssensors.8b01642
ACS Sens. 2019, 4, 717−725

REFERENCES

(1) Kho, Z. Y.; Lal, S. K. The Human Gut Microbiome—A Potential Controller of Wellness and Disease. *Front. Microbiol.* **2018**, *9*, 1.

(2) Honda, K.; Littman, D. R. The microbiota in adaptive immune homeostasis and disease. *Nature* **2016**, *535* (7610), 75—84.

(3) Zhu, W.; Winter, M. G.; Byndloss, M. X.; Spiga, L.; Duerkop, B. A.; Hughes, E. R.; Büttner, L.; Romao, E.; Behrendt, C. L.; Lopez, C. A.; et al. Precision editing of the gut microbiota ameliorates colitis. *Nature* **2018**, *553* (7687), 208—211.

(4) Althani, A. A.; Marei, H. E.; Hamdi, W. S.; Nasrallah, G. K.; Zowalaty, M. E.; Khodor, S. A.; Al-Asmakh, M.; Abdel-Aziz, H.; Cenciarelli, C. Human Microbiome and its Association With Health and Diseases. *J. Cell. Physiol.* **2016**, *231* (8), 1688—94.

(5) Yamazaki, Y.; Nakamura, Y.; Núñez, G. Role of the microbiota in skin immunity and atopic dermatitis. *Allergol. Int.* **2017**, *66* (4), 539—44.

(6) Benhadou, F.; Mintoff, D.; Schnebert, B.; Thio, H. Psoriasis and Microbiota: A Systematic Review. *Diseases* **2018**, *6* (2), 47.

(7) Langan, E.; Griffiths, C.; Solbach, W.; Knobloch, J.; Zillikens, D.; Thaci, D. The role of the microbiome in psoriasis: moving from disease description to treatment selection. *Br. J. Dermatol.* **2018**, *178* (5), 1020—7.

(8) Francuzik, W.; Franke, K.; Schumann, R. R.; Heine, G.; Worm, M. Propionibacterium acnes Abundance Correlates Inversely with Staphylococcus aureus: Data from Atopic Dermatitis Skin Microbiome. *Acta dermato-venereologica* **2018**, *98* (5—6), 490—5.

(9) Andersson, T.; et al. *Sci. Rep.*, **2019**, accepted for publication.

(10) Allhorn, M.; Arve, S.; Brüggemann, H.; Lood, R. A novel enzyme with antioxidant capacity produced by the ubiquitous skin colonizer Propionibacterium acnes. *Sci. Rep.* **2016**, *6*, 36412.

(11) Croxen, M. A.; Law, R. J.; Scholz, R.; Keeney, K. M.; Wlodarska, M.; Finlay, B. B. Recent advances in understanding enteric pathogenic Escherichia coli. *Clin. Microbiol. Rev.* **2013**, *26* (4), 822—80.

(12) Burnham, C.-A. D.; Carroll, K. C. Diagnosis of Clostridium difficile infection: an ongoing conundrum for clinicians and for clinical laboratories. *Clin. Microbiol. Rev.* **2013**, *26* (3), 604—30.

(13) van Grinsven, B.; Eersels, K.; Akkermans, O.; Ellermann, S.; Kordek, A.; Peeters, M.; Deschaume, O.; Bartic, C.; Dilien, H.; Redeker, E. S.; et al. Label-free detection of Escherichia coli based on thermal transport through surface imprinted polymers. *ACS sensors* **2016**, *1* (9), 1140—7.

(14) Ligler, F. S.; Sapsford, K. E.; Golden, J. P.; Shriver-Lake, L. C.; Taitt, C. R.; Dyer, M. A.; Barone, S.; Myatt, C. J. The array biosensor: portable, automated systems. *Anal. Sci.* **2007**, *23* (1), 5—10.

(15) Joung, C.-K.; Kim, H.-N.; Im, H.-C.; Kim, H.-Y.; Oh, M.-H.; Kim, Y.-R. Ultra-sensitive detection of pathogenic microorganism using surface-engineered impedimetric immunosensor. *Sens. Actuators, B* **2012**, *161* (1), 824—31.

(16) Ashley, J.; Shukor, Y.; D'Aurelio, R.; Trinh, L.; Rodgers, T. L.; Temblay, J.; Pleasants, M.; Tothill, I. E. Synthesis of Molecularly Imprinted Polymer Nanoparticles for α-Casein Detection Using Surface Plasmon Resonance as a Milk Allergen Sensor. *ACS sensors* **2018**, *3* (2), 418—24.

(17) Mosbach, K. Molecular imprinting. *Trends Biochem. Sci.* **1994**, *19* (1), 9—14.

(18) Vlatakis, G.; Andersson, L. I.; Müller, R.; Mosbach, K. Drug assay using antibody mimics made by molecular imprinting. *Nature* **1993**, *361* (6413), 645—647.

(19) Ashley, J.; Shukor, Y.; Tothill, I. E. The use of differential scanning fluorimetry in the rational design of plastic antibodies for protein targets. *Analyst* **2016**, *141* (23), 6463—70.

(20) Ertürk, G.; Lood, R. Bacteriophages as biorecognition elements in capacitive biosensors: Phage and host bacteria detection. *Sens. Actuators, B* **2018**, *258*, 535—43.

(21) Ertürk, G.; Hedström, M.; Mattiasson, B.; Ruzgas, T.; Lood, R. Highly sensitive detection and quantification of the secreted bacterial benevolence factor RoxP using a capacitive biosensor: A possible early detection system for oxidative skin diseases. *PLoS One* **2018**, *13* (3), e0193754.

(22) Schirhagl, R. Bioapplications for molecularly imprinted polymers. *Anal. Chem.* **2014**, *86* (1), 250—61.

(23) Wu, J.; Babadi, A. S.; Jacobsson, D.; Colvin, J.; Yngman, S.; Timm, R.; Lind, E.; Wernersson, L.-E. Low trap density in InAs/high-k nanowire gate stacks with optimized growth and doping conditions. *Nano Lett.* **2016**, *16* (4), 2418—25.

(24) Ertürk, G.; Hedström, M.; Mattiasson, B. A sensitive and real-time assay of trypsin by using molecular imprinting-based capacitive biosensor. *Biosens. Bioelectron.* **2016**, *86*, 557—65.

(25) Ertürk, G.; Özen, H.; Tümer, M. A.; Mattiasson, B.; Denizli, A. Microcontact imprinting based surface plasmon resonance (SPR) biosensor for real-time and ultrasensitive detection of prostate specific antigen (PSA) from clinical samples. *Sens. Actuators, B* **2016**, *224*, 823—32.

(26) Montheard, J.-P.; Chatzopoulos, M.; Chappard, D. JJoMS, Part C: Polymer Reviews. 2-hydroxyethyl methacrylate (HEMA): chemical properties and applications in biomedical fields. *J. Macromol. Sci., Polym. Rev.* **1992**, *32* (1), 1—34.

(27) Liu, S; Zhang, H; Dai, J; Hu, S.; Pino, I.; Eichinger, D. J.; Lyu, H.; Zhu, H. Characterization of monoclonal antibody's binding kinetics using oblique-incidence reflectivity difference approach. *MAbs* **2015**, *7*, 110—9.

(28) McGinley, K. J.; Webster, G.; Leyden, J. J. Regional variations of cutaneous propionibacteria. *Appl. Environ. Microbiol.* **1978**, *35* (1), 62—6.

(29) Sakamoto, S.; Putalun, W.; Vimolmangkang, S.; Phoolcharoen, W.; Shoyama, Y.; Tanaka, H.; Morimoto, S. Enzyme-linked immunosorbent assay for the quantitative/qualitative analysis of plant secondary metabolites. *Journal of Natural Medicines* **2018**, *72*, 1—11.

DOI: 10.1021/acssensors.8b01642
ACS Sens. 2019, 4, 717—725